PHYSICAL REVIEW A **82**, 011603(R) (2010)

Color-charge separation in trapped SU(3) fermionic atoms

Tobias Ulbricht,[1] Rafael A. Molina,[2] Ronny Thomale,[3] and Peter Schmitteckert[4]
[1]*Institut für Theorie der Kondensierten Materie, Karlsruhe Institute of Technology, D-76128 Karlsruhe, Germany*
[2]*Instituto de Estructura de la Materia, CSIC, Serrano 123, E-28006 Madrid, Spain*
[3]*Department of Physics, Princeton University, Princeton, New Jersey 08544, USA*
[4]*Institute of Nanotechnology, Karlsruhe Institute of Technology, D-76344 Eggenstein-Leopoldshafen, Germany*
(Received 16 February 2010; published 7 July 2010)

Cold fermionic atoms with three different hyperfine states with SU(3) symmetry confined in one-dimensional optical lattices show color-charge separation, generalizing the conventional spin-charge separation for interacting SU(2) fermions in one dimension. Through time-dependent density-matrix renormalization-group simulations, we explore the features of this phenomenon for a generalized SU(3) Hubbard Hamiltonian. In our numerical simulations of finite-size systems, we observe different velocities of the charge and color degrees of freedom when a Gaussian wave packet or a charge (color) density response to a local perturbation is evolved. The differences between attractive and repulsive interactions are explored and we note that neither a small anisotropy of the interaction, breaking the SU(3) symmetry, nor the filling impedes the basic observation of these effects.

DOI: 10.1103/PhysRevA.82.011603 PACS number(s): 03.75.Ss, 71.10.Pm, 05.30.Fk

One of the most intriguing effects of strong correlations in low-dimensional systems is the separation of charge and spin degrees of freedom. As a generic phenomenon, a quantum particle carrying spin and charge converts in separate spin (spinon) and charge (holon) excitations with generally different velocities. On a microscopic bare level, there are rare examples where this process can be exactly studied in terms of explicit spinon and holon wave functions, as is the case for the Kuramoto-Yokoyama model [1–3]. However, on a low-energy effective-field-theory level, spin-charge separation (SCS) manifests itself in a generic one-dimensional interacting system belonging to the Luttinger liquid (LL) universality class, where spinons and holons are described by independent collective excitations [4]. Despite several attempts, the *direct* observation of SCS has proved elusive [5]. So far, the best experimental evidence is provided by tunneling between quantum wires where interference effects relate to excitations with different velocities [6].

Since recently, one possible avenue for the observation of SCS is ultracold Bose or Fermi gases confined in optical lattices. There, the interaction parameters and dimensionality can be tuned with high precision by means of an atomic Feshbach resonance or by changing the depth of the wells in an optical lattice [7]. Several theoretical works have addressed the possibility of observing SCS in cold-fermionic gases [8–13] and in cold-bosonic gases [14] with two internal degrees of freedom. Thanks to the special properties of cold atomic systems, these theoretical proposals could address previously unexplored features of SCS, such as the problem of the breaking of the SU(2) symmetry and the description of SCS at high energies. In particular, higher spin fermions can be directly studied with cold atoms in more than two hyperfine states. These kinds of systems could give rise to new phases in optical lattices due to the emergence of triplets and quartets (three- or four-fermion bound states) and other phenomena [15–23]. At least the two alkali-metal atoms ^{6}Li and ^{40}K are possible candidates for the experimental realization of an SU(3) fermionic lattice with attractive interactions [18]. In the case of ^{6}Li the scattering lengths for the three possible channels of the three lowest lying hyperfine levels ($|F,m\rangle = |1/2,1/2\rangle$, $|1/2,-1/2\rangle$, and $|3/2,-3/2\rangle$) at large magnetic fields become similar at a scattering length of $a_s \approx -2500a_0$ [24]. Moreover, the realization of a stable and balanced three-component Fermi gas has been recently reported to potentially accomplish both an attractive and repulsive regime with approximate SU(3) symmetry [25,26]. The scattering lengths of the different channels for the three lowest hyperfine states of ^{40}K near the Feshbach resonance were also measured. In addition, the possibility of trapping them optically was demonstrated [27].

It is the purpose of this work to use time-dependent density-matrix renormalization-Group (TD-DMRG) [28–32] simulations to study the phenomenology of color-charge separation (CCS) in lattice systems with three different kinds of fermions, where the color notation is inherited from the quark description of high-energy SU(3) theories of quantum chromodynamics. As one of the quantities to be obtained from TD-DMRG, the different color and charge velocities are extracted from time-dependent simulations and compared to a low-energy LL approach.

The low-energy physics of cold fermionic atoms with three different hyperfine states trapped in an optical lattice can be described by an SU(3) version of the Hubbard Hamiltonian:

$$H = -t \sum_{\langle ij\rangle,\alpha} (f^\dagger_{i\alpha} f_{j\alpha} + \text{H.c.}) + \sum_{i,\alpha\neq\beta} \frac{U_{\alpha\beta}}{2} n_{i\alpha} n_{i\beta}. \quad (1)$$

The sums α and β extend over the three colors red (r), green (g), and blue (b) corresponding to three different hyperfine states. The operators $f^\dagger_{i\alpha}$ and $f_{i\alpha}$ are the creation and destruction operators of an atom on site i with color α. We consider different values of the on-site interaction between the different color pairs $U_{\alpha\beta}$ to be able to include SU(3) symmetry-breaking terms. The site label i goes from 0 to $L-1$, with L being the total number of lattice sites corresponding to the wells forming the optical lattice. For cold atoms, there is an additional harmonic confinement term that arises due to the Gaussian profile of the laser beams. If this trap potential is weak, we can assume to be located in the trap center where the confinement can be considered constant. In the following calculations we

ignore the confinement, since the SU(2) spin-charge separation persists in a trap [13].

The hopping term can be controlled by varying the depth of the wells through the laser intensity. The optical lattice potential that each of the hyperfine states is affected by is very similar and the hopping rates can be considered equal for the three different spin species (colors). In the rest of the article, all energies are expressed in units of $t \equiv 1$. The interaction strength in each channel is proportional to the corresponding s-wave scattering length $U_{\alpha\beta} = 4\pi\hbar^2 a_{\alpha\beta}/m$. We do not take into account the population of higher bands and spin-flipping rates because in experiments these are usually negligible [33].

In the linear bosonization approach, being valid in the weak-coupling limit, the low-energy effective theory of the model can be expressed in terms of the collective fluctuations of densities of the three spin species plus charge density. Introducing three bosonic fields $\phi_\alpha(x)$ and assuming that the position x is measured in units of the distance between sites, the density operators for each color can be written as

$$\rho_{i,\alpha} \approx \bar{\rho} + \frac{1}{\sqrt{\pi}}\partial_x\phi_\alpha(x) - \frac{1}{\pi}\sin\left[2k_F x + \sqrt{4\pi}\phi_\alpha(x)\right], \quad (2)$$

where k_F is the Fermi wave-vector and x corresponds to the lattice site. We express the bosonized Hamiltonian in terms of a total density described by a charge field,

$$\Phi_{\rm ch} = \frac{1}{\sqrt{3}}\sum_\alpha \phi_\alpha, \quad (3)$$

and the relative spin densities described by two bosonic fields,

$$\Phi_3 = \frac{1}{\sqrt{2}}(\phi_r - \phi_b) \quad \text{and} \quad \Phi_8 = \frac{1}{\sqrt{6}}(\phi_r + \phi_b - 2\phi_g). \quad (4)$$

The subindices were chosen to correspond to the SU(3) group Casimir operators J_3 and J_8. For an SU(3) symmetric Hamiltonian, the model can be separated into a charge and a color part, $H = H_{\rm ch} + H_{\rm col}$,

$$H_{\rm ch} = \frac{v_{\rm ch}}{2}\left[\frac{1}{K}(\partial_x\Phi_{\rm ch})^2 + K(\partial_x\Theta_{\rm ch})^2\right], \quad (5)$$

where $v_{\rm ch} = v_F/K$ is the density velocity, $K = (1 + 2U/\pi v_F)^{-1/2}$ is the LL parameter, $\Theta_{\rm ch}$ is the conjugate field of the bosonic field $\Phi_{\rm ch}$, and

$$H_{\rm col} = \sum_{\mu=3,8}\left\{\frac{v_F}{2}[(\partial_x\Phi_\mu)^2 + (\partial_x\Theta_\mu)^2] - \frac{U}{2\pi}(\partial_x\Phi_\mu)^2\right\} + \frac{U}{2\pi^2}\cos\sqrt{2\pi}\Phi_3\cos\sqrt{6\pi}\Phi_8 - \frac{U}{2\pi^2}\cos\sqrt{8\pi}\Phi_3. \quad (6)$$

Similarly, the color velocity is approximated as $v_{\rm col} = v_F\sqrt{1 - U/(\pi v_F)}$. However, due to the nonlinear cosine terms in (6), we do not expect a linear relation between distance and time for color excitations to hold for long times. If SU(3) symmetry is not strictly observed there appear mixing terms coupling density and color degrees of freedom. A renormalization group analysis of this model can elucidate the low-energy properties of the system [34,35]. The most important difference with respect to the SU(2) case is that for $U \gtrsim 0$, umklapp processes present for commensurate fillings do not open a gap in the charge sector. We expect a phase transition between the MI and the LL at a finite value of U. In fact, with Monte Carlo calculations, Assaraf *et al.* [34] estimated the critical interaction scale at $U_{\rm cr} = 2.2$, while recent DMRG calculations suggest the critical point to be much closer to zero [36]. The cosine terms for the color Hamiltonian are irrelevant for repulsive but relevant for attractive interaction and are responsible for a gap opening in the color sector in the attractive case.

We now explain how the CCS appears in real-time simulations of SU(3) spin chains. We study the time evolution of the Hamiltonian (1) with the TD-DMRG algorithm [10,29]. We find the number of states needed to keep sufficient accuracy during the time evolution to be >7000. Such huge demands limit the system size we can simulate to $L = 18$ for periodic boundary conditions (PBC) and to $L = 48$ for hard-wall boundary conditions (HWBC), which is settled in the range of present state of the art limits. For the small systems, the finite-size effects are large. However, comparable simulations on SU(2) systems provide the detailed knowledge that the effects are rather independent of interaction parameters. Comparison with exact results for $U = 0$ of the charge and color velocities provide approximations to the Luttinger liquid parameter, which we use as a tuning point to compare field theory and numerical results.

We show snapshots of the time evolution for different interaction strengths in Fig. 1 for the system with $L = 18$ and PBC. We calculate the ground-state $|\Psi_0\rangle$ of the SU(3) Hamiltonian (1) with $N = 27$ fermions. Then, we put an extra (green) fermion with an initial wave packet in the system that travels to the right with a finite momentum centered around $k = 0.6\pi$,

$$|\Psi^{+1}(T=0)\rangle = \sqrt{\frac{\pi}{2\sigma^2}}\sum_x e^{(ikx)}e^{-\frac{(x-x_0)^2}{2\sigma^2}} f^\dagger_{x,\rm green}|\Psi_0\rangle, \quad (7)$$

and a width of $\sigma = 1.5$. Choosing $N = 27$ leads to an average density of $\overline{\langle n\rangle} = 1.5$ and an incommensurate filling of $\nu = 0.5$, the commensurate fillings being $\nu = 1/3$ and $2/3$. Time is always measured in inverse units of the hopping

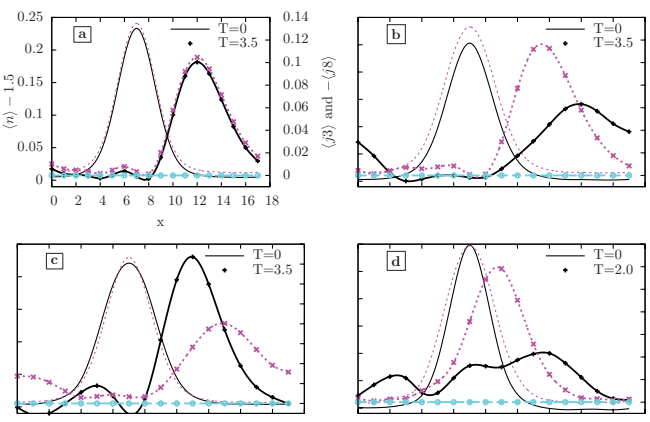

FIG. 1. (Color online) Snapshots of the time evolution of an additional fermion for filling $\nu = 0.5$ and $U = 0$ (a), $U = +1$ (b), $U = -1$ (c), and $U = +5$ (d). The initial state is a Gaussian wave packet with average momentum $k = 0.6\pi$. In panels (b)–(d), the color density of the quantum number j^8 (magenta dotted line) separates from the charge density (black solid line).

rate. The panels in the figure show the particle density $\langle n\rangle = \langle\Psi^{+1}(T)|\sum_\alpha f_\alpha^\dagger f_\alpha|\Psi^{+1}(T)\rangle$ and the corresponding densities of the color quantum numbers j^3 and j^8 relative to the uniform ground-state density at the initial time and at a finite time. We observe a slight dispersion effect [Fig. 1(a)] due to the finite width of the wave packet. Moreover, the velocity of the excitation is not exactly the velocity of a plane wave with momentum k. In Fig. 1(b), for the case $U = 1$, we see the separation of density and color degrees of freedom. The initial excitation separates and the color and charge density evolve with different velocities. The decay of the charge-density excitation is more rapid for strong repulsive interaction as it is seen in the case $U = 5$, indicating the opening of the charge gap. In similar ways, a gap in the color sector should open for attractive interaction and spoil the color-density evolution in that regime. However, in our example with $U = -1$, we can still observe rather clean and stable CCS since, for the finite system, the arising gap in the color sector is too small to reasonably detect an enhanced color excitation decay. To extract color and charge velocities, we applied two different extraction methods. First, the velocity can be obtained by dividing the number of sites traveled by the maximum of the density by the time. It is more accurate to fit a Gaussian on the density for every time step. There is a short transient time at the beginning, followed by a plateau of constant velocity until the packet hits the boundary. We extract the velocity of the packet when it passes the median between the initial position and the boundary and take a Gaussian-averaged value around this position. As a second measure, for a definite plateau of constant velocity, we use an $L = 48$ sites system with HWBCs and replace the incident electron by an initial, small potential perturbation. The time development of this method differs mainly by the implicit stimulation of excited states around both Fermi points. This leads to symmetric peaks running in both directions and increasing the transient time at the start. Figure 2 shows snapshots of the initial time and a finite time step for $U = 1.5$, where the perturbation is taken to be the derivative of a Gaussian and is fitted for the two propagating wave packets. We find that both methods provide similar results, while the latter proves to be a considerable improvement in precision and is put forward by us as a generally preferable method to extract velocities from TD-DMRG.

Finally, the extracted velocities are shown as a function of the uniform interaction in Fig. 3 using the latter method. On top of the data, we show the expected relation for $v_{\rm col}(U), v_{\rm ch}(U)$

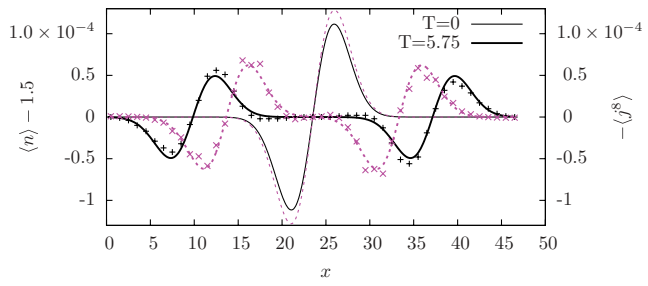

FIG. 2. (Color online) Snapshots of a perturbation at time $T = 0$ (thin lines) and a finite time step (thick lines and data points). The dashed (solid) lines are fits to the color density of j^8 (charge density n) with the corresponding data points.

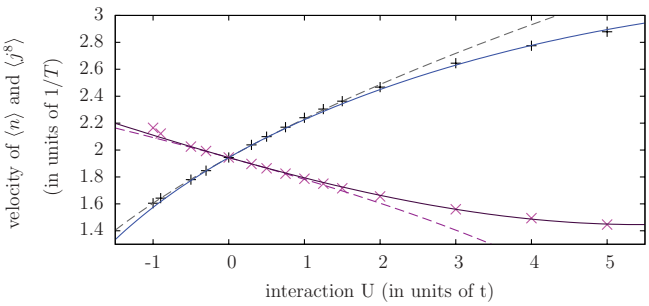

FIG. 3. (Color online) Velocity $v(U)$ of an initial Gaussian perturbation. Results of our TD-DMRG simulations for both charge density (+) and color density (×). The dashed lines represent bosonization results, scaled to match the DMRG velocity at $U = 0$. The solid lines are fits on a next-to linear dependency in U.

from bosonization, scaled to match the free fermion velocity. This *a priori* renormalization covers all direct effects that lead to deviations of the Fermi velocity due to finite width or the central momentum k_0 of the excitation and the finite-size dispersion. Even for $|U|$ up to 1, the agreement between the bosonization estimate and the numerical data is found to be excellent (dashed lines in Fig. 3). Moreover, the limits of applicability of the low-energy expansion are reached. However, upon extending the velocity expansion to higher order in U, with $v_{\rm ch} = v_F\sqrt{1 + 2U/(\pi v_F) + aU^2}$, the fit already covers the complete computed range in U (solid line in Fig. 3) and the parameter $a = -0.017$ has the same order and sign as the fit by Assaraf *et al.* [34] who chose a different filling in their Monte Carlo simulations. Similarly, we obtain a fit for $v_{\rm col} = v_F\sqrt{1 - U/(\pi v_F) + bU^2}$ with $b = 0.015$.

A possible candidate for realizing the trionic phase ($U < 0$) is ^{6}Li for which the magnetic field dependence of the three scattering lengths has been measured [24]. The attractive U interaction for magnetic fields around 1000 G can be estimated as $U_{rg} = U_0$, $U_{rb} = 1.23U_0$, and $U_{gb} = 1.06U_0$, due to the ratios in the s-wave scattering rate in each channel [24]. It is important to consider whether these anisotropies infringe on the validity of the effects observed. In bosonization theory, anisotropy introduces new terms that couple the charge and color degrees of freedom so we would expect that high anisotropies destroy charge-color separation [35]. However, small and experimentally accessible anisotropies turn out to be not decisively important. We have checked that the separation effect of color and charge densities remains without much change. Even for the special cases of commensurate fillings where a stronger sensitivity on the color anisotropy may have been suspected, the qualitative behavior persists.

In summary, we have performed TD-DMRG simulations of cold fermionic atoms with three hyperfine states trapped in an optical lattice. We have prepared the system in the ground state and added a fermionic Gaussian wave packet with a definite momentum or disturbed the initial ground state by adding a Gaussian potential. Our simulation allowed us to observe the color-charge separation in SU(3) fermionic systems in a generic non-commensurate case. We have obtained the charge and color velocities as a function of the interaction from the real-time simulations for both the attractive and

the repulsive case. Once we take into account finite-size effects by renormalizing the noninteracting velocities, our results at weak coupling are in good agreement with the LL calculations.

The authors acknowledge discussions with Philippe Lecheminant and Stephan Rachel. R.A.M. is supported in part by MICINN (Spain) Grant No. FIS2009-07277, and R.T. is supported by the Humboldt Foundation. Parts of the DMRG calculations have been performed on an HP XC4000 at Steinbuch Center for Computing (SCC) Karlsruhe under Project RT-DMRG. We acknowledge the support by the Center for Functional Nanostructures (CFN), Project B2.10.

[1] B. A. Bernevig, D. Giuliano, and R. B. Laughlin, Phys. Rev. B **65**, 195112 (2002).
[2] R. Thomale, D. Schuricht, and M. Greiter, Phys. Rev. B **74**, 024423 (2006); **75**, 024405 (2007).
[3] Y. Kuramoto and H. Yokoyama, Phys. Rev. Lett. **67**, 1338 (1991).
[4] T. Giamarchi, *Quantum Physics in One Dimension*, *International Series of Monographs on Physics* (Oxford University Press, Oxford, 2004).
[5] M. Bockrath *et al.*, Nature (London) **397**, 598 (1999); P. Segovia, D. Purdie, M. Hengsberger, and Y. Baer, *ibid.* **402**, 504 (1999); R. Losio *et al.*, Phys. Rev. Lett. **86**, 4632 (2001); T. Lorenz *et al.*, Nature (London) **418**, 614 (2002)
[6] O. M. Auslaender *et al.*, Science **308**, 88 (2005).
[7] M. Lewenstein *et al.*, Adv. Phys. **56**, 243 (2007).
[8] C. Kollath, U. Schollwöck, and W. Zwerger, Phys. Rev. Lett. **95**, 176401 (2005).
[9] C. Kollath and U. Schollwöck, New J. Phys. **8**, 220 (2006).
[10] T. Ulbricht and P. Schmitteckert, EPL **86**, 57006 (2009).
[11] P. Schmitteckert and G. Schneider, in *High Performance Computing in Science and Engineering '06*, edited by W. E. Nagel, W. Jäger, and M. Resch (Springer, Berlin, 2006), p. 113.
[12] P. Schmitteckert, in *High Performance Computing in Science and Engineering '07*, edited by W. E. Nagel, D. B. Kröner, and M. Resch (Springer, Berlin, 2007), p. 99.
[13] T. Ulbricht and P. Schmitteckert, EPL **89**, 47001 (2010).
[14] A. Kleine, C. Kollath, I. P. McCulloch, T. Giamarchi, and U. Schollwock, Phys. Rev. A **77**, 013607 (2008).
[15] C. Wu, Phys. Rev. Lett. **95**, 266404 (2005).
[16] P. Lecheminant, E. Boulat, and P. Azaria, Phys. Rev. Lett. **95**, 240402 (2005).
[17] H. Kamei and K. Miyake, J. Phys. Soc. Jpn. **74**, 1911 (2005).
[18] A. Rapp, G. Zaránd, C. Honerkamp, and W. Hofstetter, Phys. Rev. Lett. **98**, 160405 (2007).
[19] C. Honerkamp and W. Hofstetter, Phys. Rev. Lett. **92**, 170403 (2004).
[20] A. V. Gorshkov *et al.*, Nat. Phys. **6**, 289 (2010).
[21] S. Rachel, R. Thomale, M. Fuhringer, P. Schmitteckert, and M. Greiter, Phys. Rev. B **80**, 180420 (2009).
[22] B. Errea, J. Dukelsky, and G. Ortiz, Phys. Rev. A **79**, 051603 (2009).
[23] R. A. Molina, J. Dukelsky, and P. Schmitteckert, Phys. Rev. A **80**, 013616 (2009).
[24] M. Bartenstein *et al.*, Phys. Rev. Lett. **94**, 103201 (2005).
[25] T. B. Ottenstein, T. Lompe, M. Kohnen, A. N. Wenz, and S. Jochim, Phys. Rev. Lett. **101**, 203202 (2008).
[26] J. H. Huckans, J. R. Williams, E. L. Hazlett, R. W. Stites, and K. M. O'Hara, Phys. Rev. Lett. **102**, 165302 (2009).
[27] C. A. Regal, Ph.D. thesis, University of Colorado, 2005 [http://jila.colorado.edu/pubs/thesis/regal/].
[28] S. R. White, Phys. Rev. Lett. **69**, 2863 (1992).
[29] P. Schmitteckert, Phys. Rev. B **70**, 121302(R) (2004).
[30] A. J. Daley, C. Kollath, U. Schollwöck, and G. Vidal, J. Stat. Mech. (**2004**) P04005.
[31] S. R. White and A. E. Feiguin, Phys. Rev. Lett. **93**, 076401 (2004).
[32] U. Schollwöck, Rev. Mod. Phys. **77**, 259 (2005).
[33] D. Jaksch, C. Bruder, J. I. Cirac, C. w. Gardiner, and P. Zoller, Phys. Rev. Lett. **81**, 3108 (1998).
[34] R. Assaraf, P. Azaria, M. Caffarel, and P. Lecheminant, Phys. Rev. B **60**, 2299 (1999).
[35] P. Azaria, S. Capponi, and P. Lecheminant, Phys. Rev. A **80**, 041604 (2009).
[36] K. Buchta, O. Legeza, E. Szirmai, and J. Sólyom, Phys. Rev. B **75**, 155108 (2007).